Q. J. R. Meteorol. Soc. (1997), **123**, pp. 1653–1675

The role of the environmental flow in the development of secondary frontal cyclones

By IAN A. RENFREW[1]*, ALAN J. THORPE[2] and CRAIG H. BISHOP[3]

[1] *University of Toronto, Canada*
[2] *University of Reading, UK*
[3] *Pennsylvania State University, USA*

(Received 10 April 1996; revised 10 October 1996)

SUMMARY

The impact of the environmental flow on the development of secondary frontal cyclones is investigated. Several case-studies are examined as examples of secondary frontal-cyclone events observed in the North Atlantic–western Europe sector. A simple measure of growth is defined to chart their development. The vorticity attribution technique of Bishop is utilized to calculate the action of the large-scale (environmental) flow on the fronts. In particular the environmental along-front stretching—shown to be important in theoretical models of frontal instabilities—is calculated. The role of the environmental deformation appears to be crucial: as part of a baroclinic life cycle, stretching deformation acts to build up a front but suppress along-front waves; if the stretching rate diminishes, barotropic instabilities may then break out. Diagnostics are examined to try to ascertain the growth mechanisms at work in each frontal-cyclone case. A range of values for the commonly prescribed deformation-frontogenesis and shearing-frontogenesis parameters are calculated.

KEYWORDS: Barotropic development Deformation Frontogenesis Vorticity attribution

1. INTRODUCTION

The downstream tail of the North Atlantic synoptic storm track appears to be the area most energetic in terms of subsynoptic-scale cyclonic activity (Ayrault *et al.* 1995). One subset of these subsynoptic cyclones is that of secondary frontal cyclones, defined as waves on the pre-existing frontal zones of primary cyclonic systems. Such secondary frontal cyclones are an important and common local-forecasting problem in western Europe, especially as they occasionally deepen explosively into full-blown storms (e.g. Hoskins and Berrisford 1988). Ordinary secondary frontal cyclones (those that do not deepen explosively) are typically up to 1000 km in scale, fast-growing and short-lived (lifetimes of 1–2 days), see Hewson (1993) and Ayrault *et al.* (1995). Figure 1 shows one such frontal cyclone (L_{R1}) marked on the trailing cold front of a synoptic-scale low-pressure system south of Greenland. This is an interesting case as two frontal cyclones develop, the one indicated and a second 12 hours later. The two cyclones appear similar in size and structure initially, but their evolutions are decidedly different: an explanation for this difference is put forward in section 3.

Theoretical modelling studies have found instabilities on the above length-scales and time-scales if the frontal zone includes a low-level extremum in potential vorticity (Joly and Thorpe 1990; Malardel *et al.* 1993; Polavarapu and Peltier 1993); or equivalently a boundary potential-temperature anomaly (Schär and Davies 1990; Joly 1995†). These situations are unstable to barotropic or internal baroclinic instabilities via the Charney–Stern (1962) instability criterion. The wave amplification can be thought of in terms of a phase locking and mutual amplification of edge waves on the edges of the potential-vorticity strip or warm band (see, for example, Hoskins *et al.* (1985)). However, when the

* Corresponding author: Department of Physics, University of Toronto, 60 St George Street, Toronto, Ontario, M5S 1A7, Canada.

† Note that in Joly (1995) frontal waves were also found to amplify transiently, without a boundary potential-temperature anomaly.

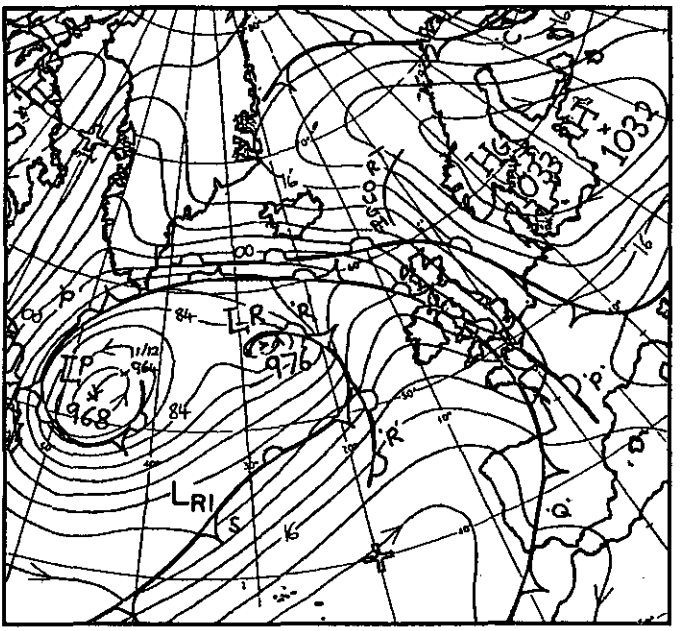

Figure 1. Mean-sea-level pressure map at 12 GMT 12 November 1994 for the North Atlantic sector—redrawn from the UK Meteorological Office manual analysis. Isobars are every 4 mb and lines of latitude and longitude are every 10°. The frontal cyclone (L_{RI}) is indicated on the cold front of parent cyclone L_R.

action of the environmental flow (i.e. the baroclinic wave in which the front is embedded) is included, this is also found to be crucial to any frontal-wave development. For example, in Thorncroft and Hoskins (1990) the most unstable modes (about 1000 km in scale) were torn apart when added to a baroclinic life-cycle experiment.

The two most important environmental flow mechanisms instrumental in forming and intensifying fronts are those of horizontal shearing and horizontal deformation. Several recent studies have examined the impact of these two frontogenesis mechanisms on the development of along-front waves. Joly and Thorpe (1991) investigated the growth of disturbances on a horizontal-shearing-forced front. For moist frontogenesis there was the possibility of rapid frontal cyclogenesis dependent upon two factors: the rate of frontogenesis and the state of the parent baroclinic wave. The authors suggest that the direct action of horizontal shearing deformation does not affect frontal-wave growth; but indirectly larger shearing frontogenesis leads to a front with greater potential instability.

Bishop and Thorpe (1994a, b, hereafter BT94I and BT94II) specifically investigated barotropic edge-wave growth on an idealized moist tropospheric front in an external deformation flow. It was found that wave amplification depended upon the magnitude of the potential vorticity (PV) of the strip and the scale of the disturbance relative to the strip width. While the deformation flow and induced ageostrophic convergence act (via latent-heat release) to increase the PV of the strip, they also tend to flatten nascent frontal waves. Furthermore, the deformation-frontogenesis process changes the non-dimensional wave length of the waves through time—pushing them out of the 90° phase shift required for maximum amplification. Hence, there is a trade-off between keeping the waves in phase for as long as possible and keeping the waves in phase when the PV of the strip is large and waves will amplify more rapidly. A stretching-deformation rate of greater than 0.6×10^{-5} s^{-1} suppresses most wave growth, at all scales; whereas a lower deformation

rate of (for example) 0.2×10^{-5} s^{-1} allows large amplification of frontal cyclone-scale waves.

A highly idealized study by Dritschel *et al.* (1991) examined the role of external horizontal deformation and external horizontal shearing on edge-wave growth. Of the two they found the suppressing action of the external deformation flow was the primary effect. The role of deformation on baroclinic instabilities is less clear-cut—see Bishop (1993a, b).

It is clear from the above studies that both a potential for frontal instability and the evolving environmental flow are decisive in the development of any along-front waves. So, for a proper analysis of observational data, both the potential instability and the action of the environmental flow must be examined. The difficulty is that obtaining the relevant information from the complicated observational data is fraught with problems: for example, the local structure of the front masks the action of the environmental flow on the front. To compare the real atmosphere to theoretical models one really needs a way of partitioning the observed flow into, ideally, a *frontal* part and an *environmental* (background) part. This would allow a comparison between the front and its environment in both the real atmosphere and a theoretical model. In other words, such a partition would allow an analogy between the potential instability and its environment, and the perturbation and basic-state parts of theoretical models. The two separate parts could then be analysed individually and relevant diagnostics calculated.

One way to achieve this partition is by using an *attribution technique*, where an anomaly is isolated and a particular flow field is associated with, or attributed to, that anomaly in some coherent manner. Utilizing such a technique in a practical way has been the subject of some research (e.g. Hoskins *et al.* 1985; Davis and Emanual 1991; Davis 1992; Bishop and Thorpe 1994c). The technique used in this study is that of domain-independent vorticity and divergence attribution developed by Bishop (1996a, b). This technique is summarized in section 2. Using domain-independent attribution allows the accurate calculation of the environmental stretching-deformation rate which is shown to be crucial to frontal-wave development in theoretical studies. In section 3 the relationship between frontal-cyclone growth and the environmental stretching deformation is investigated for a variety of real case-studies. Section 4 synthesizes the results of all the case-studies, the aim being to provide a quantitative relationship between stretching deformation and frontal-cyclone growth. Section 5 concludes the paper.

2. Analysis techniques

(a) *Domain-independent attribution*

A horizontal wind field on a periodic or global domain can be uniquely partitioned* into *irrotational* and *non-divergent* parts (Helmholtz theorem, see Morse and Feshbach (1953) for example). So, for a horizontal wind, $\mathbf{u}$,

$$\mathbf{u} = -\nabla \times (\psi \mathbf{k}) + \nabla \chi = \mathbf{u}_\psi + \mathbf{u}_\chi, \tag{1}$$

with stream function ψ and velocity potential χ, where $\mathbf{k}$ is the unit vector in the vertical. So $\mathbf{u}_\psi$ is non-divergent and $\mathbf{u}_\chi$ is irrotational. Defining the vertical component of the vorticity

* Note that here the *partitioning* problem is that of separating a given wind field into irrotational and non-divergent parts as described, for example, in Lynch (1988). The word 'partition' is also used in a more general sense elsewhere to mean the division of a wind field in some way. Closely related is the *reconstruction* problem which concerns the calculation of a wind field from given vorticity and divergence distributions (with winds given at the domain boundaries).

as $\xi = \mathbf{k} \cdot \nabla \times \mathbf{u}$ and the divergence as $\delta = \nabla \cdot \mathbf{u}$, then combining these and (1), leads to the Poisson equations:

$$\nabla^2 \psi = \xi \text{ and } \nabla^2 \chi = \delta. \tag{2}$$

So the non-divergent part of the wind $\mathbf{u}_\psi$ is due to the vorticity distribution, and the irrotational part of the wind $\mathbf{u}_\chi$ is due to the divergence distribution.

It is well known that such a unique partition is *not* possible on a finite domain, where the partition depends upon the boundary conditions imposed (e.g. Lynch 1988, 1989). The approach of Bishop (1996a) bypasses this problem by solving the Poisson equations (2) using *free-space* Green's functions, i.e. where the boundary conditions are removed to infinity. This introduces a certain domain independence to the solutions. In two dimensions the Green's function is $\ln(r)$, where r is the radial distance from the centre of the disc, so the induced winds are proportional to $1/r$. For discrete data in a finite domain, a unique wind field is attributed to each element of vorticity and divergence by calculating the wind field due to a disc of uniform vorticity and divergence assigned to each grid point in the domain. The vorticity and divergence of the discs are calculated via sophisticated circulation and flux estimates using wind data from the neighbouring grid points. To obtain the total *rotational* flow $\mathbf{u}_\psi$ (the flow due to all the vorticity in the finite domain) the wind induced by all the vorticity-grid discs is summed. To obtain the total *divergent* flow $\mathbf{u}_\chi$ the winds induced by all the divergence-grid discs are summed. As the domain is finite there is also a remainder flow: the *harmonic* part of the wind, $\mathbf{u}_\vartheta$, defined by

$$\mathbf{u}_\vartheta = \mathbf{u} - \mathbf{u}_\psi - \mathbf{u}_\chi. \tag{3}$$

The harmonic wind is both solenoidal and irrotational in the domain, and so can be represented as a stream function ($\mathbf{u}_\vartheta = -\nabla \times \vartheta \mathbf{k}$) or velocity potential ($\mathbf{u}_{\vartheta'} = \nabla \vartheta'$). It can be calculated independently by solving

$$\nabla^2 \vartheta = 0 \text{ in the interior,} \quad \text{subject to } \frac{\partial \vartheta}{\partial n} = \mathbf{n} \cdot \mathbf{u}_\vartheta, \tag{4}$$

where $\mathbf{n} \cdot \mathbf{u}_\vartheta$ is calculated via (3) on the finite-domain boundary. So the attribution technique allows a unique and unambiguous three-component partition of the wind vector, $\mathbf{u}_{\text{obs}}$, on a finite domain that is independent of the domain boundaries thus:

$$\mathbf{u}_{\text{obs}} = \mathbf{u}_\psi + \mathbf{u}_\chi + \mathbf{u}_\vartheta. \tag{5}$$

The rotational part of the wind is due to vorticity, the divergent part due to divergence, and the harmonic part due to vorticity and divergence outside the domain. Hence, there is a clear relationship between a vorticity or divergence distribution and the wind field induced by it.

The details of the adaptation of the technique into a discrete formulation suitable for limited areas of gridded wind data are described by Bishop (1996a). Note that the reconstruction of the wind field can be achieved to a high degree of accuracy: root-mean-square and maximum wind errors are typically 0.1 m s^{-1} and 0.25 m s^{-1} respectively.

(*b*) *Frontal flow and environmental flow*

The attribution method allows the association of a particular wind field to each grid-point element of vorticity and divergence, so one can partition (or divide) a wind field by partitioning the vorticity and divergence distributions. In other words, one can specify a particular region of the domain and examine the flow due to vorticity and divergence in

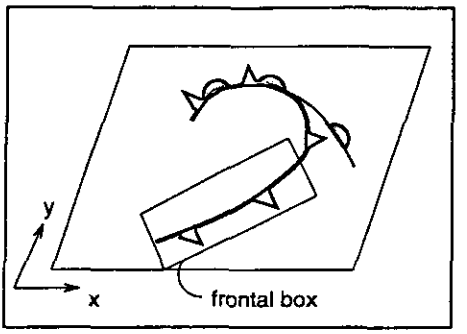

Figure 2. A schematic of a frontal box defined for a synoptic low.

that region only. Following the ideas of Bishop (1996b) one can 'draw a box around' a cold front (Fig. 2) and define the *frontal* flow as the wind induced by vorticity and divergence inside the box, and the *external* or *environmental* flow as the wind induced by vorticity and divergence external to the frontal box (including vorticity and divergence outside the finite domain). Hence there is a division of the wind field into these two distinct parts:

$$\mathbf{u}_{\text{obs}} = \mathbf{u}_{\text{e}} + \mathbf{u}_{\text{i}} = (\mathbf{u}_{\text{e}\psi} + \mathbf{u}_{\text{e}\chi} + \mathbf{u}_{\vartheta}) + (\mathbf{u}_{\text{i}\psi} + \mathbf{u}_{\text{i}\chi}), \tag{6}$$

where $\mathbf{u}_{\text{e}}$ is the wind due to vorticity and divergence external to the frontal region (rotational + divergent + harmonic parts) and $\mathbf{u}_{\text{i}}$ is the wind due to vorticity and divergence inside the frontal region (rotational + divergent parts).

So, to investigate the impact of the large-scale flow on a front one would examine the environmental wind, $\mathbf{u}_{\text{e}}$. This wind is due to vorticity and divergence distant from the front and so would be expected to be relatively smooth in the frontal region. It is this division into frontal and environmental flows that allows a comparison between real and theoretical-model fronts, and their division into perturbation parts and balanced basic states. In our partition the environmental wind is due to the synoptic system (and other surrounding systems) within which the front is embedded, and the frontal wind is due to the front and any waves on the front. The prescribed *frontal box* may be defined as any shape: it is simply defined by the grid points that are inside the box (frontal) and those that are outside (environmental). In this study the frontal box is defined to enclose the strip of positive vorticity that typically delineates a baroclinic frontal zone, with the box edges parallel to the strip. So, for fronts and frontal waves, the box used is either a rectangle or a segment of an annulus, thus covering both straight and curved fronts. At subsequent times the position of the frontal box is moved (and slightly elongated if necessary) so that the frontal wave is consistently enclosed.

To calculate the magnitude of the deformation flow shown to be crucial to modelled frontal-wave development (Dritschel *et al.* 1991; BT94II), the along-front stretching due to the environmental flow is measured by $\partial v_{\text{e}}/\partial y_{\text{f}}$. Note there is a rotation of coordinates into a frontal coordinate system, so $(x_{\text{f}}, y_{\text{f}})$ are the (across-front, along-front) directions respectively. The along-front direction is defined as parallel to the frontal-box sides, or as the arc through the centre of the frontal annulus. The across-front direction points towards the warm air for a cold front. Note that for convenience the subscript f on the velocity is dropped but that the subscript on the coordinate is retained.

As discussed by Bishop (1996b), if the stretching of the observed winds is used to estimate the deformation rate serious errors may occur. Firstly the local structure of the

front will cause along-front waves in the stretching pattern, and secondly a small variation in angle can cause a large change in stretching rate (due to the large shear associated with the front). Calculating stretching from the environmental winds dramatically reduces these errors by 'removing' the frontal shear. A sensitivity study in Renfrew (1995), where the frontal-box size and angle were varied by ±25% in width and ±3° in angle, found a variation of only 3% in $\partial v_e/\partial y_f$ from the prescribed deformation rate in an idealized front, and only 0.06×10^{-5} s^{-1} (10%) from the original-box estimate in a real-data case. This can be compared to variations of 15% and 0.25×10^{-5} s^{-1}, respectively, in calculating $\partial v_{obs}/\partial y_f$.

(c) *A measure of frontal-wave amplitude*

A key issue is how to measure the size and growth of an observed frontal wave. Most analytical studies (e.g. Dritschel *et al.* 1991; BT94I and BT94II) use the amplification of the wave slope as a measure of growth, as it is proportional to the amount of nonlinear growth. Essentially the wave slope is the angle between an isoline of vorticity (for example) and its basic-state position, i.e. on a horizontal plane $\partial\xi/\partial y_f$. Unfortunately, defining and calculating wave slope in real data have large associated errors. To be measurable, the wave slope must be defined relative to some 'undisturbed' frontal position, and in observed fronts this undisturbed position is a conjectural matter. Ideally the measure of growth should be relatively insensitive to the chosen along-front direction. However, as wave slope is defined relative to this direction it is intrinsically directly dependent upon it.

To overcome this problem, a new measure of along-front variation has been developed starting from a practical, observational perspective rather than a theoretical one. The new measure of growth is the *peak vorticity* minus the *maximum along-front average vorticity* of the strip:

$$W(\xi) = \xi_{peak} - \max\{\bar{\xi}^y\}, \tag{7}$$

where y is the along-front direction. The peak vorticity is simply the maximum value in a specified frontal region (i.e. the frontal box). To compare this peak value with the strength of the front, the along-front average vorticity for each column of grid points in the frontal box is calculated, and the maximum of these is subtracted from ξ_{peak} to obtain $W(\xi)$. We have called $W(\xi)$ the *vorticity waviness*. The main advantages of $W(\xi)$ are that it is straightforward to calculate in observed flows, and does not depend directly on the along-front direction—it depends only indirectly through the along-front average term. It appears from the real-data sensitivity studies by Renfrew (1995) that $W(\xi)$ is relatively insensitive to small changes in the along-front direction as such changes give variations less than 0.06×10^{-4} s^{-1} (8%) from the original-box value. Vorticity waviness is a simpler measure than wave slope, which means it should be less affected by small-scale noise. However, it is sensitive to model resolution (as are all vorticity measures) and to the length of the frontal region specified. Care needs to be taken that this vorticity-strip length is defined consistently through the instability evolution—another reason for a 'Lagrangian' approach to defining the frontal box.

In Renfrew (1995) instabilities of a strip of vorticity in a numerical barotropic vorticity-equation model are investigated, the results being similar to Dritschel *et al.* (1991). The amplitudes of the instabilities are measured using both wave slope and vorticity waviness, and these measures are shown to be comparable through the evolution of the frontal instability. This result provides some justification for the use of $W(\xi)$ on real data and interpreting the results in the context of other analytical work.

3. Case-studies

A series of frontal-cyclone case-studies was investigated and the results are outlined below. A broad range of events was chosen, and each case exhibits distinctive features. However, a detailed description of each case is beyond the scope of this paper and instead the reader is referred to Renfrew (1995). The key goals in the investigation are:

- measuring the growth of the frontal wave,
- examining the environment of the front in suppressing or allowing frontal-wave growth,
- suggesting probable growth mechanisms on the basis of calculated diagnostics, and
- measuring key parameters usually prescribed in frontal theory, i.e. the deformation rate, α, and the horizontal shearing-frontogenesis parameter, s^2 (cf. Hoskins and Bretherton 1972).

The data used in this study are analyses from the UK Meteorological Office Unified Limited Area Model (LAM); this is described in detail by Cullen (1993) and the references within. Analyses are processed four times daily at 00 GMT, 06 GMT, 12 GMT and 18 GMT; note this is also local time for the United Kingdom in each case. The Unified Model (LAM version) is run operationally at a resolution of 0.44° latitude (approximately 50 km grid resolution) with 19 vertical levels. Unfortunately, the data are downgraded to a 100 km resolution for archiving purposes.

Clearly the analyses generated give only an incomplete representation of the atmosphere at any time. There will be processes occuring at subgrid-scales which will not be resolved by the model, and there will be errors in the resolved structures due to data-collection errors and to approximations made in the model formulation. Secondary frontal waves in the range 500–1000 km in scale are close to the limit of what can be confidently represented in the LAM, especially in their development stage. Indeed it seems inevitable that there will be some errors in data assimilation at various times and that these could cause inaccurate forecasts. This may have been the source of the poor forecast of 1–2 February 1994 (see section 3(*b*)). On the positive side, one recent innovation has been the routine assimilation of remotely sensed surface-wind data over the oceans, determined via a scatterometer on the ERS-1* satellite (Bell 1994). This has improved data coverage over the otherwise data-sparse Atlantic Ocean.

In each of the following cases the LAM analyses are taken as 'true' with some reservation, given the above limitations. We are confident that the larger-scale disturbances are well represented and that overall trends (growth and decay) of mesoscale systems are well represented, even if the precise details are not. So there is little doubt in our conclusions in each case; however, some of the values of, for example, vorticity waviness may not be exact. Note that the attribution calculation of environmental along-front stretching relies on the environmental winds being well represented. These are due mainly to the larger-scale vorticity and divergence patterns, rather than the local structure, and this is well represented in general, so the environmental along-front stretching of the fronts will be accurately calculated.

(*a*) *Case (a): 12–13 November 1994*

Figure 1 shows the mean-sea-level pressure analysis for 12 GMT 12 November 1994, where a frontal cyclone (L_{R1}) with a weak pressure signature is analysed. A second frontal cyclone (L_{R2}) is subsequently analysed on the same frontal zone, south-west of the first. Initially the two frontal cyclones appear to have largely similar characteristics and be of

* European Remote Sensing.

similar horizontal size and depth. For example, examination of the potential vorticity at 900 mb shows the front defined by a PV strip approximately 0.4 PVU greater than the surrounding area at 00 GMT 12 November (when the first frontal cyclone, L_{R1}, develops) and the same at 00 GMT 13 November (when the second, L_{R2}, develops). Other diagnostics such as low-level vorticity and temperature gradients also appear similar for the two waves. However, the two frontal cyclones develop in markedly different ways. On 12 November L_{R1} increases rapidly in terms of vorticity waviness, $W(\xi)$, as seen in the vorticity plots (Figs. 3(a) and 3(b)) at 00 GMT and 12 GMT (12 November) and in Fig. 5. L_{R2} does not have such an increase in $W(\xi)$, but becomes less wavy and more two-dimensional on 13 November.

The hypothesis was that L_{R1} and L_{R2} were being affected in different ways by their environments. To calculate the environmental flow on the front, a 'frontal box' was defined at each time, and the external induced winds calculated (i.e. those induced by vorticity and divergence external to the frontal box) as described in section 2. The frontal boxes enclosing L_{R1} at 00 GMT and 12 GMT (12 November), and enclosing L_{R1} and L_{R2} at 00 GMT (13 November), are outlined in bold in Fig. 3. Figure 4 shows contours of along-front stretching and wind vectors for the 00 GMT frontal box: (a) for the observed winds, $\mathbf{u}_{obs}$, and (b) for the environmental winds, $\mathbf{u}_e$. Note there is a great deal of small-scale structure in the $\partial v_{obs}/\partial y_f$ field even at this early time when L_{R1} is not that significant; the $\partial v_e/\partial y_f$ field is much smoother and more uniform, giving an accurate representation of the background stretching-deformation rate (the average over the central half of the box is 0.8×10^{-5} s^{-1}). There are noticeable 'end effects' in the environmental stretching due to the cutting of the frontal vorticity strip (by the prescribed frontal box) causing extraneous circulations in the frontal region. By averaging over the centre of the domain their impact can be neglected (see Renfrew (1995) for a longer discussion).

The above analysis was carried out for the 30-hour period of investigation and the results are plotted in Figs. 5 and 6. Figure 5 shows vorticity waviness $W(\xi)$ and the along-front average vorticity (a measure of frontal strength) and Fig. 6 shows the environmental stretching $\partial v_e/\partial y_f$ for both L_{R1} and L_{R2}. The vorticity waviness of L_{R1} increases dramatically from 00 GMT to 12 GMT 12 November, then drops off slowly as the frontal cyclone equilibrates. As shown in nonlinear frontal-cyclone simulations (e.g. Schär and Davies 1990; Malardel *et al.* 1993), if a frontal cyclone remains barotropic, the instability will quickly saturate and the wave will equilibrate. This appears to have happened for L_{R1}—it is not deep enough to move into a baroclinic-growth phase. The rapid increase in $W(\xi)$ is coincident with a steady decrease in environmental along-front stretching of the front. The initially large $\partial v_e/\partial y_f$ average of 0.8×10^{-5} s^{-1} has halved to 0.4×10^{-5} s^{-1} by 12 GMT and is negative by 00 GMT 13 November. In the idealized model of BT94II, sustained along-front stretching greater than 0.6×10^{-5} s^{-1} strongly inhibits frontal-wave growth. The observed environmental stretching on L_{R1} falls below this value at about 06 GMT. Over the following 6 hours, $W(\xi)$ increases dramatically. Thus, in this case, the observations are qualitatively and quantitatively consistent with their theoretical model. The data for L_{R1} concord with the hypothesis that a weakening environmental-stretching rate allows the frontal wave to grow. The data for L_{R2} concord with the converse of this hypothesis—that is, if the environmental stretching remains large (around 1×10^{-5} s^{-1} through to 06 GMT 13 November) then the frontal wave cannot develop.

To confirm this scenario, along-front profiles of the environmental stretching were plotted; $\partial v_e/\partial y_f$ was calculated by averaging over the central few grid points of a longer frontal box enclosing both L_{R1} and L_{R2} at 00 GMT (cf. Fig. 3(c)) and 06 GMT 13 November. These show a geographical variation in the environmental stretching along the front—L_{R1} was in a low stretching regime (around -0.2×10^{-5} s^{-1}) and L_{R2} was in a high

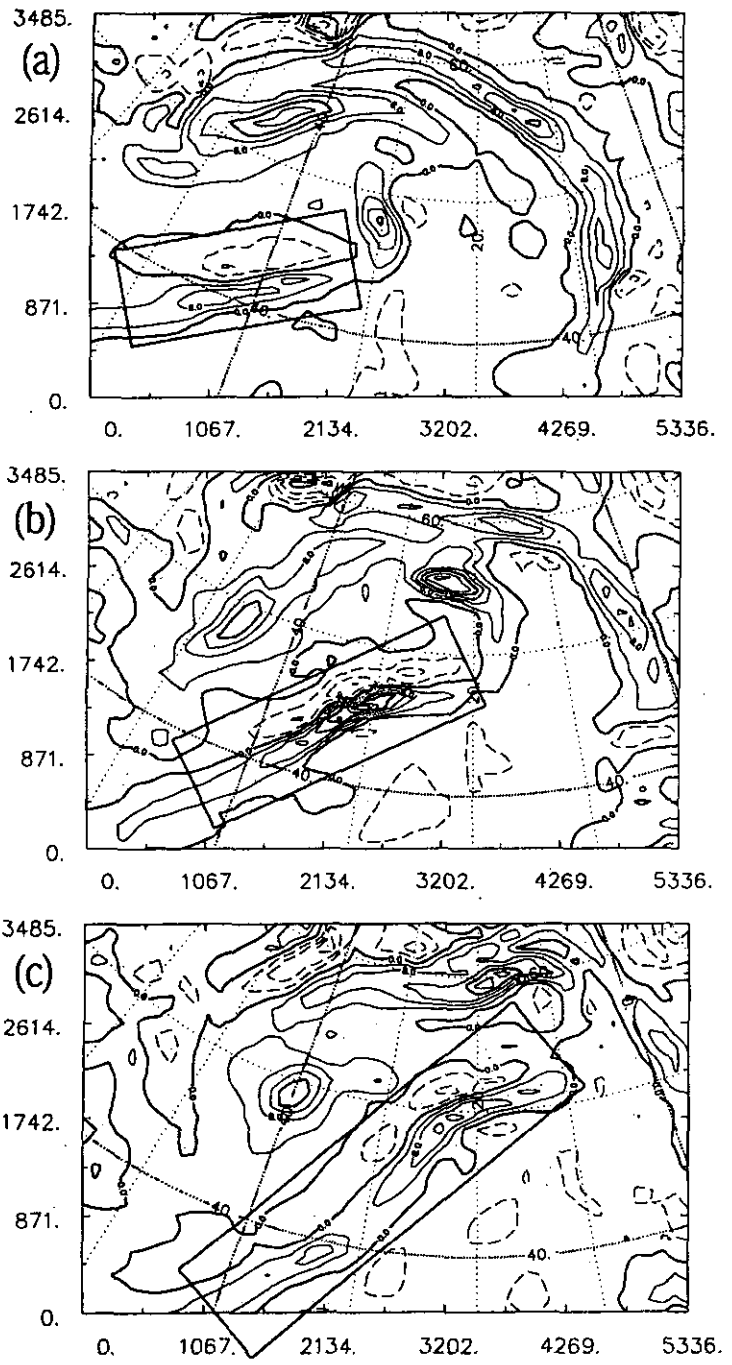

Figure 3. Relative-vorticity plots at (a) 00 GMT and (b) 12 GMT 12 November 1994 and (c) 00 GMT 13 November 1994, at the 900 mb level: (a) and (b) show L_{R1} in the frontal box (outlined in bold) and (c) shows L_{R1} and L_{R2}. The contour interval is 0.4×10^{-4} s^{-1}, with negative values shown dashed, with lines of latitude and longitude drawn every 10° and with the axes labelled in km.

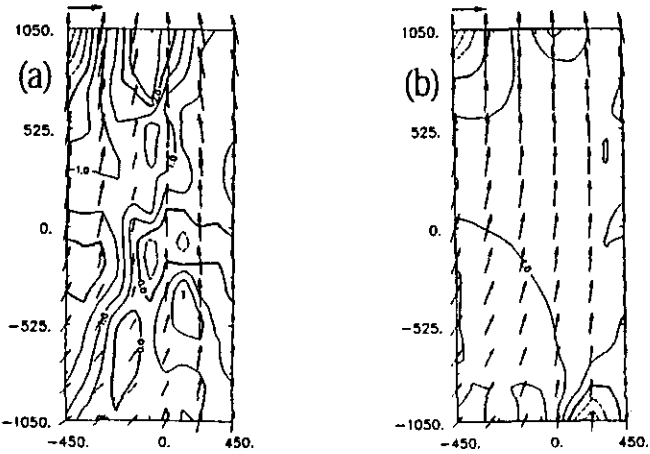

Figure 4. Contours of along-front stretching for (a) the observed winds and (b) the environmental winds, at 00 GMT 12 November 1994, for the frontal box indicated in Fig. 3(a). Also shown are vectors of the corresponding winds, i.e. $\mathbf{u}_{obs}$ and $\mathbf{u}_e$ respectively. The contour interval is 0.5×10^{-5} s^{-1} and the scaling arrows for the winds are 28 m s^{-1}. The axes labelling is in km.

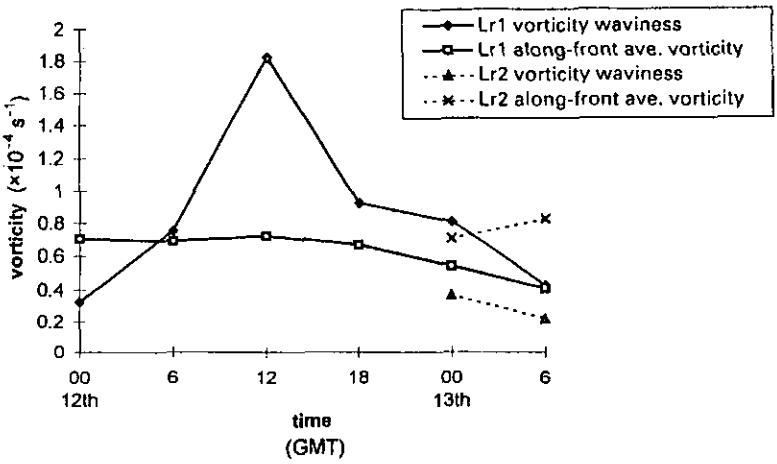

Figure 5. Vorticity waviness and the maximum along-front average vorticity for the 30-hour period of investigation of L_{R1} and L_{R2} of case (a) (see text). The along-front average vorticity is over the full frontal box.

stretching regime (around 0.8×10^{-5} s^{-1})—the difference being due to their different locations relative to the synoptic systems. These different stretching regimes could certainly account for the different evolutions, indeed they concur with the barotropic edge-wave modelling results of BT94II.

To check whether L_{R1} was growing through barotropic edge-wave dynamics, derivatives of the perturbation-wind field can be examined. The barotropic nature of frontal waves means that diagnostics such as pressure, stream function or temperature are swamped by the basic state (cf. BT94II, Fig. 8). Using the attribution method makes it possible to plot the observed-wind equivalent of the theoretical perturbation-wind derivatives. It should be noted that only the derivatives of the perturbation winds are compared. The partition of the observed-wind field into frontal ($\mathbf{u}_i$) and environmental ($\mathbf{u}_e$) parts is (for practical

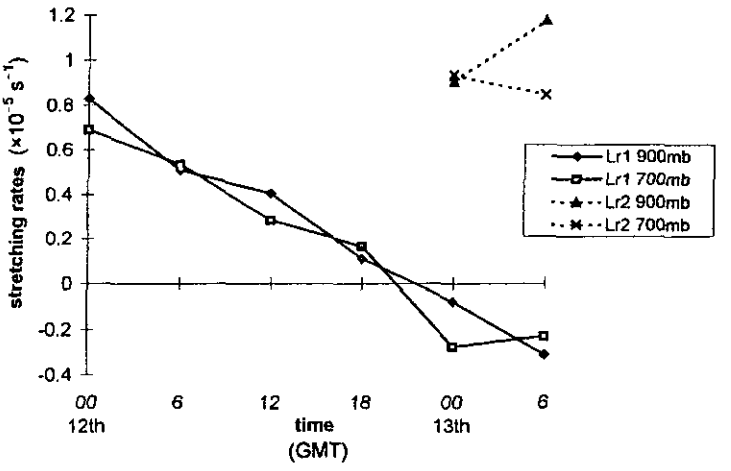

Figure 6. Along-front environmental-stretching rates at the 900 mb and 700 mb levels for L_{R1} and L_{R2} of case (a) (see text). The plotted values are averages over the central half of the frontal box.

reasons) not the same as the partition used in the theoretical studies of BT94II. The observed frontal winds ($\mathbf{u}_i = \mathbf{u}_{i\psi} + \mathbf{u}_{i\chi}$) include the frontal-wave velocities and the frontal velocities, whereas in BT94II the perturbation winds are only the frontal-wave velocities—the front is part of the basic state. However, when taking along-front derivatives of $\mathbf{u}_i$ the frontal part is removed, as its along-front derivatives are zero, and so a comparison with theory is valid. Figure 7 shows $\partial v_i/\partial y_f$ and $\partial u_i/\partial y_f$ for 12 GMT and 18 GMT 12 November. Comparing the v-derivatives with Fig. 10 of BT94II reveals that the patterns are remarkably similar. The real-data $\partial v_i/\partial y_f$ tilt with the shear, and over about $1\frac{1}{2}$ wavelengths are similar to the idealized patterns; there is other 'noise' but the comparison is reasonably convincing. Comparing the u-derivatives (with Fig. 9 in BT94II) the patterns are less convincing. The cross-front wind is weaker and the derivative pattern is more diffuse. At 12 GMT $\partial u_i/\partial y_f$ patterns are not that similar, but at 18 GMT the real-data pattern is more like the theoretical pattern. It is likely that, at the earlier time, the signature of the weaker cross-front wind component is being masked by other noise; later the cross-front flow is stronger and the pattern is more obvious. It does seem that barotropic processes are playing an important part in the development of L_{R1}.

Throughout the period the exterior induced horizontal shear, $\partial v_e/\partial x_f$, is negative (i.e. adverse to the shear of the vorticity front). It falls from around -0.3×10^{-5} s^{-1} at 00 GMT 12 November to about zero at 00 GMT 13 November (for the 900 mb level). This decrease in environmental shear implies less suppression of barotropic instabilities (Dritschel 1989; Dritschel *et al.* 1991). However, for the shears calculated here (and indeed in all the other tropospheric fronts investigated) this is very much a secondary factor.

In summary: L_{R1} moved from an area of strong to an area of weak environmental along-front stretching, coincidently with a period of rapid growth of the frontal cyclone. This increase in amplitude appears to be due to barotropic edge-wave growth. In contrast L_{R2} remained in an area of strong environmental stretching and did not amplify: the growth mechanism was suppressed by the configuration of the synoptic systems. The geographical distribution of stretching deformation was thus crucial in determining the different frontal-cyclone evolutions.

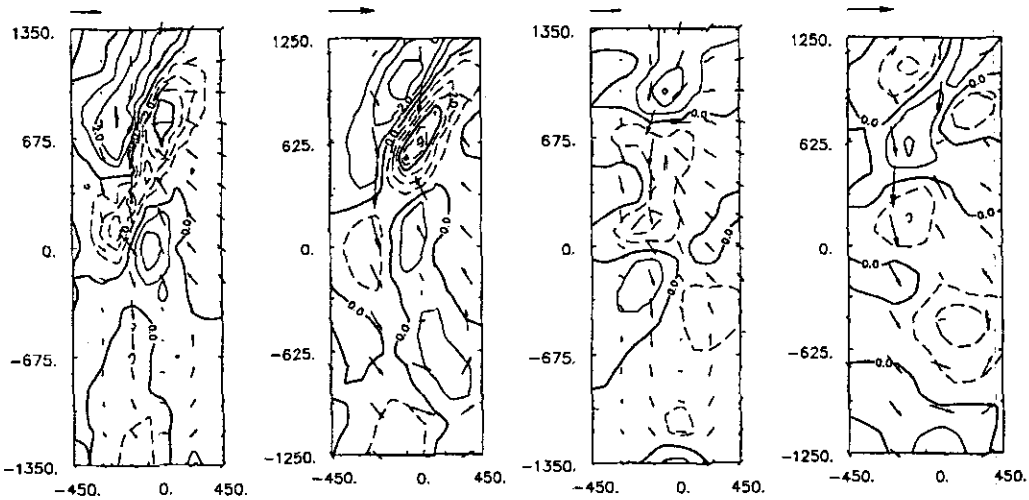

Figure 7. Contours of the along-front frontal-induced wind derivatives, $\partial v_i/\partial y_f$ (left) at 12 GMT and 18 GMT 12 November 1994, and $\partial u_i/\partial y_f$ (right) at 12 GMT and 18 GMT 12 November 1994 (see text for explanation of symbols). The vectors are the corresponding $\mathbf{u}_i$ winds. The contour interval is 1×10^{-5} s^{-1} with negative values shown dashed and the scaling arrow is 15 m s^{-1}. The frontal box for 12 GMT is as shown in Fig. 3(b). The axes labelling is in km.

(*b*) *Case (b): 1–2 February 1994*

At 18 GMT 1 February 1994 (Fig. 8) a number of frontal cyclones are shown on a wavy cold front extending across northern Europe and the North Atlantic. Two of these, L_Q and L_R, are shown with closed isobars and appear to be approximately the same size and magnitude. However, their subsequent evolutions are totally different: L_Q remains an ordinary frontal cyclone with surface pressure staying around 1000 mb before eventually saturating, whereas L_R deepens explosively (47 mb in 42 hours) into a full-blown storm. This is a particularly interesting case as the UK Meteorological Office 36-hour forecast was very poor, missing the explosive growth of L_R and instead deepening both L_Q and L_R to a moderate extent and putting them at different locations (see Renfrew 1995).

It was hypothesized that the different evolutions of the two frontal cyclones may have been due to different environmental flows, so the attribution technique was used to investigate the period from 00 GMT 1 February to 12 GMT 2 February. On investigation it was found that both frontal cyclones were undergoing weak stretching deformation during 1–2 February (L_Q negative, around -0.2×10^{-5} s^{-1}, and L_R positive, at $0–0.3 \times 10^{-5}$ s^{-1}). These values are well below the critical mark of BT94II, and so barotropic instabilities should be free to grow. Parker (1996, personal communication) examines the effects of negative stretching on barotropic instabilities, and finds rapid but transient growth is possible. An examination of the Bishop (1993b) f_1 case (for a mid-latitude baroclinic zone, cf. his Figs. 2 and 3) indicates this magnitude of strain also has a negligible effect on baroclinic growth. Thus the calculated environmental stretching should allow either (or both) L_Q and L_R to grow barotropically or baroclinically; so it appears that it is not the action of the environmental flow that makes the crucial difference in their developments.

The rapid deepening and the increase in scale of L_R signifies a transition from a barotropic growth process to a baroclinic one (see Malardel *et al.* 1993). To grow baroclinically L_R must be large enough in scale to 'feel' the baroclinicity on the dynamical tropopause, i.e. the horizontal scale must be larger than the Rossby radius (Malardel *et al.*

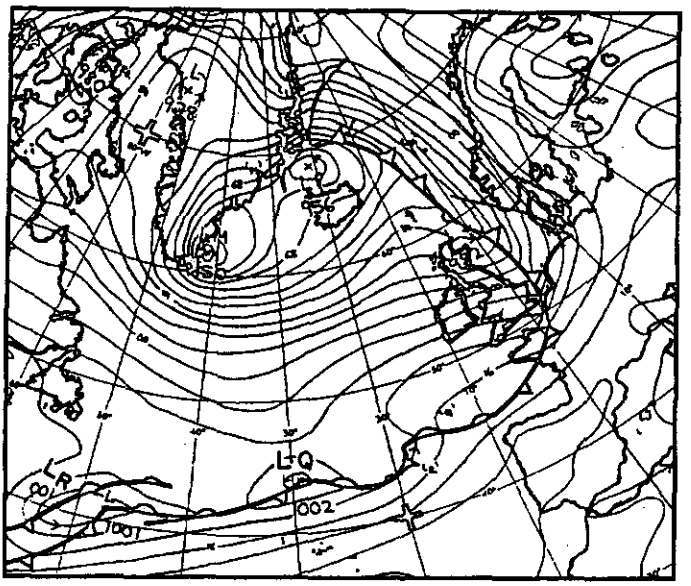

Figure 8. Mean-sea-level pressure map at 18 GMT 1 February 1994 for the North Atlantic sector—redrawn from the UK Meteorological Office manual analysis. Isobars are every 4 mb. Frontal cyclones L_Q and L_R are analysed with closed isobars at this time.

1993). A close examination of the size and depth of the two frontal cyclones, from pressure and vorticity diagnostics, reveals that L_R was marginally larger than L_Q. For example, along-front cross-sections of PV (e.g. 12 GMT 2 February, see Fig. 9) illustrate that L_Q was too shallow to phase-lock with a tropopause undulation, whereas L_R was deep enough to phase-lock with a more pronounced tropopause fold. Isentropic advection of PV from the stratosphere into the lower troposphere would thus allow a rapid deepening of L_R. This fits the scenario put forward by Thorncroft and Hoskins (1990) to explain the explosive growth of frontal cyclones: upper-level reinforcement of a low-level anomaly. Note that, although this explanation fits the available data, as discussed earlier the data are not perfect; and, given the poor forecast, some caution must be expressed about the exact details of the growth mechanisms at work in this particular case.

The lack of large-scale horizontal deformation motivates the comparison of this case with the horizontal shearing-frontogenesis model of Joly and Thorpe (1991). Calculations of the *along-front* temperature gradient due to the large-scale flow were made via a 2-level balance approach (see the appendix). It was found that the along-front temperature gradient was not particularly strong on average. For example, using the 900 mb and 700 mb levels, the along-front temperature gradient due to the environmental flow was about 0.1 K per 100 km at L_R, and -0.2 K per 100 km at L_Q, at 18 GMT 1 February. This would imply a small value of the horizontal shearing-frontogenesis parameter, s^2, (Hoskins and Bretherton 1972) for this time. In the Eady problem, and in horizontal shearing-frontogenesis models, a typical value of s^2 is taken to correspond to an along-front gradient of ± 0.5 to 1 K per 100 km. The slow frontogenesis implied here would favour the amplification of 1000 km scale waves in the shearing-frontogenesis model of Joly and Thorpe (1991). From these 1000 km scale waves it seems that one of them, L_R, becomes large enough to couple with a pronounced tropopause undulation and to deepen explosively, whereas the other, L_Q, saturates through nonlinear processes.

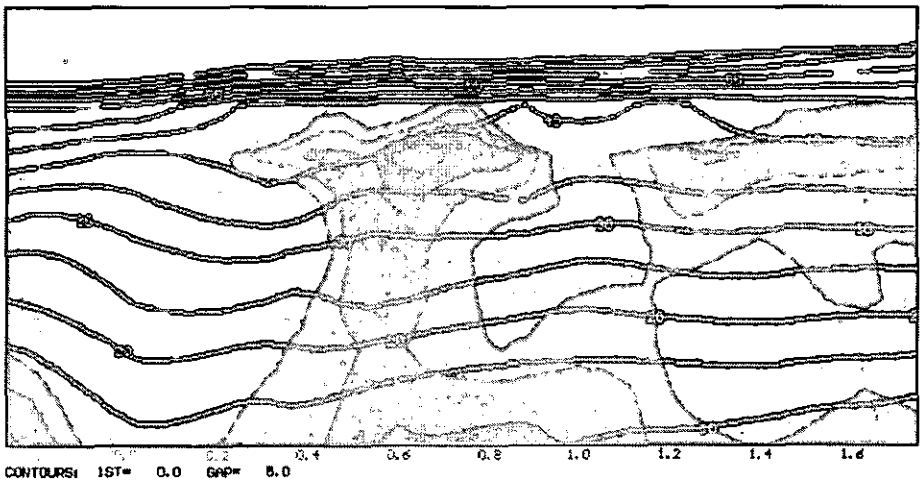

Figure 9. A cross-section of potential vorticity (shading) and isentropes (contours) along the elongated front, passing through L_R (left) and L_Q (right) at 12 GMT 2 February 1994. The shading indicates PV values at an interval of 0.2 PVU from −0.2 to 1.6; the isentropes are every 5 K as labelled.

(c) *Case (c): 26 November 1994*

The 26 November case was reminiscent of a classic Bergeron deformation-forced front; the pressure analysis (Fig. 10) indicates a low-level confluence flow on the front trailing southwards from L_L (954 mb). The front was shallow but had a well defined signature in low-level vorticity (Fig. 11), potential temperature and also PV (magnitude 1 PVU at 900 mb), so instabilities of the type modelled by Joly and Thorpe (1990) and Schär and Davies (1990) would be possible. However, the along-front stretching due to the environmental flow was calculated to be extremely strong: deformation rates were between 1.2 and 1.6×10^{-5} s^{-1} for the 900 mb and 700 mb $\mathbf{u}_e$ winds (00 GMT to 12 GMT). These are larger than the 1×10^{-5} s^{-1} value usually prescribed in frontogenesis theory, and significantly greater than the critical values of BT94II.

From the BT94II model it is actually possible to calculate a minimum strain rate (α_{min}) necessary to suppress *all* barotropic frontal-wave growth. For a valid comparison to be made it is necessary to check that the observed case and the idealization are alike. Therefore, diagnostics of moist PV and relative humidity were examined to confirm that the front was close to moist neutrality ($PV_e \approx 0$) and saturated (the relative humidity was over 95%). Hence the following equation could be employed:

$$\alpha_{min} = \frac{f}{4}\left(\frac{\zeta_4 - \zeta_2}{\zeta_4 + \zeta_2}\right) e^{-2\mu}, \tag{8}$$

where ζ_4 is the absolute vorticity of the strip, ζ_2 is the absolute vorticity of the neighbouring anticyclonic region and 2μ is the non-dimensional wave number of the disturbance. Taking $\zeta_4 = f + 1.0 \times 10^{-4}$ s^{-1} and $\zeta_2 = f - 0.3 \times 10^{-4}$ s^{-1} (Fig. 11), with $f = 1.0 \times 10^{-4}$ s^{-1}, setting $2\mu = 0$ (i.e. an infinite wavelength) then sets an upper limit for α_{min}, so at 00 GMT $\alpha_{min} = 1.2 \times 10^{-5}$ s^{-1} for complete wave suppression. The measured value of $\partial v_e/\partial y_f'$ is 1.6×10^{-5} s^{-1}, so on this front the theory predicts that all waves should be suppressed. Note that, in reality, 2μ is non-zero and instead the wavelength of any instability is limited by the width and length of the vorticity strip. An estimate of these at 00 GMT gives a width

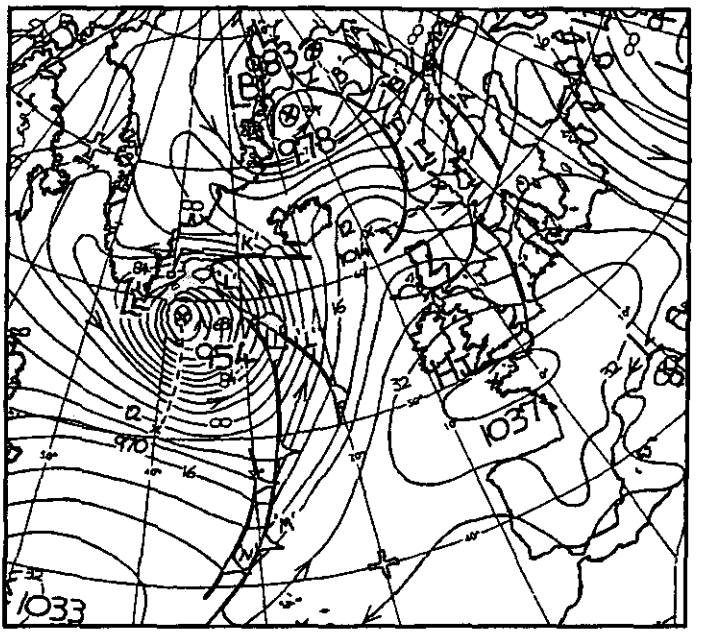

Figure 10. Mean-sea-level pressure map at 00 GMT 26 November 1994 for the North Atlantic sector—redrawn from the UK Meteorological Office manual analysis. Isobars are every 4 mb. The cold fronts of L_L that are examined are labelled 'M' and 'N'.

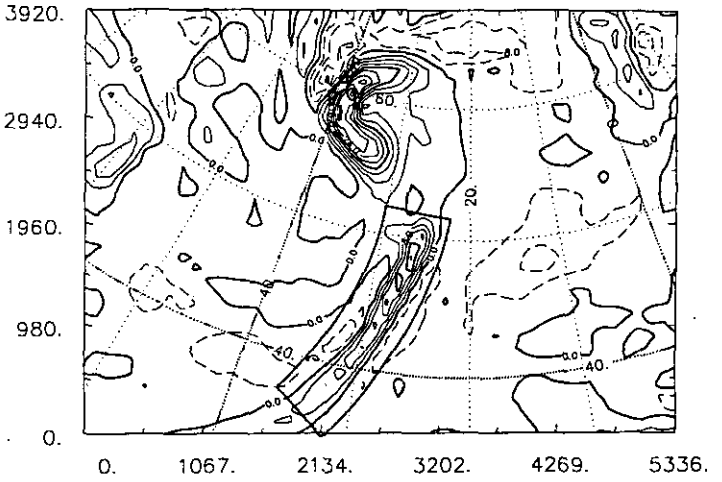

Figure 11. Relative vorticity at 900 mb for 00 GMT 26 November 1994. The frontal box (see Fig. 3) is outlined in bold and the contour interval is 0.4×10^{-4} s^{-1} with negative values shown dashed. The axes labelling is in km.

of 250 km and a length of 2500 km, so $e^{-2\mu} = 0.63$ and $\alpha_{min} = 0.75 \times 10^{-5}$ s^{-1} (less than half the measured rate). However, one must also consider that the magnitude of the vorticity of the frontal strip will not be fully resolved in the forecast model. If the relative vorticity of the strip is doubled ($\zeta_4 = f + 2.0 \times 10^{-4}$ s^{-1}), then α_{min} would be 0.98×10^{-5} s^{-1} for the estimated strip dimensions—also much less than the measured rate.

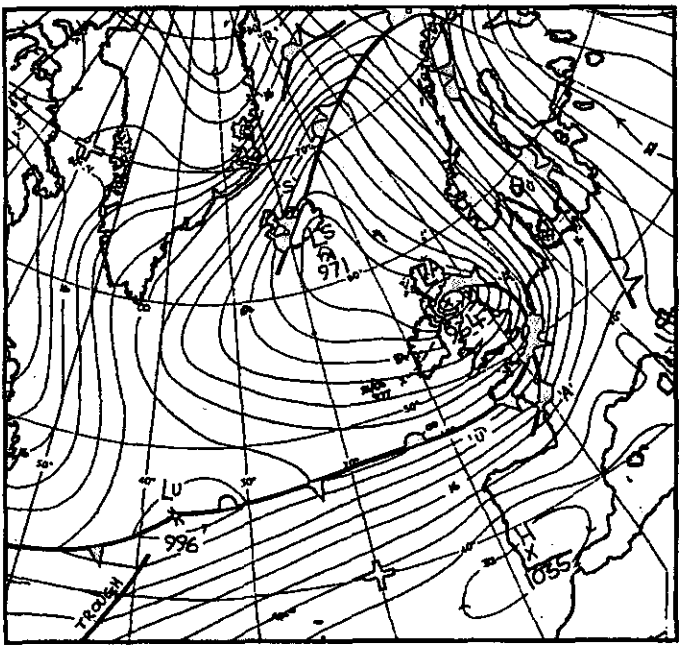

Figure 12. Mean-sea-level pressure map at 18 GMT 21 January 1995 for the North Atlantic sector—redrawn from the UK Meteorological Office manual analysis. Isobars are every 4 mb. Frontal cyclone L_A, now a parent cyclone, and L_U, a col wave on its cold front, are labelled.

Over the next 12 hours the front remains fairly two-dimensional, $W(\xi)$ decreases from 0.7×10^{-4} s^{-1} at 00 GMT to 0.3×10^{-4} s^{-1} at 12 GMT, so, as predicted, wave growth is suppressed by the strong deformation flow.

(*d*) *Case (d): 20–22 January 1995*

A common scenario observed in the North Atlantic sector is when a mesoscale secondary cyclone 'runs around' the southern flank of a parent synoptic-scale cyclone (the 'Icelandic Low') and then deepens as it moves into the parent system, eventually becoming a parent cyclone itself (e.g. Browning and Roberts 1994; Browning *et al.* 1995). This scenario occurred four times in succession in January 1995 and two of these events are investigated here.

Figure 12 shows a mean-sea-level pressure analysis at 18 GMT 21 January 1995; L_A has moved around L_S and is now a parent cyclone, with a col wave L_U growing on its front. L_A shadowed an upper-level PV tongue, and only deepened when the tongue moved over a low-level baroclinic zone at about 00 GMT 21 January. L_U was primarily a low-level feature with a strong low-level PV strip (1.2 PVU at 00 GMT 21 January, see Renfrew 1995), but with the added complication of a meandering upper-level tropopause anomaly (marked as a trough on Fig. 12) which also seemed to play a role in the low-level growth.

Figure 13 shows $W(\xi)$ and the along-front average vorticity over the period, for both L_A and L_U. There is an increase in $W(\xi)$ and along-front average vorticity for L_A around 00 GMT 21 January, coincident with the movement of the upper PV tongue over the low-level baroclinic zone. Hence, the growth process is envisaged as primarily a baroclinic interaction between the upper tongue and the low-level baroclinicity, similar to that modelled by Thorncroft and Hoskins (1990). Initially there is not a strong enough low-level PV strip at

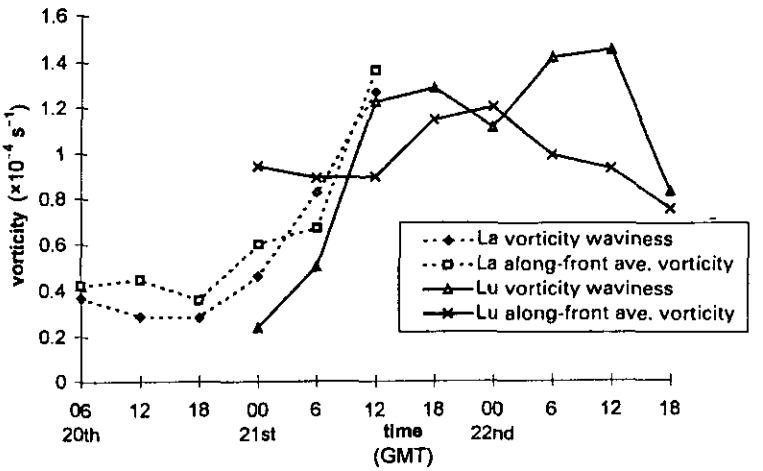

Figure 13. Vorticity waviness and the maximum along-front average vorticity for the 60-hour period of investigation of L_A and L_U of case (d) (see text). The along-front average is taken over individual frontal boxes for each cyclone.

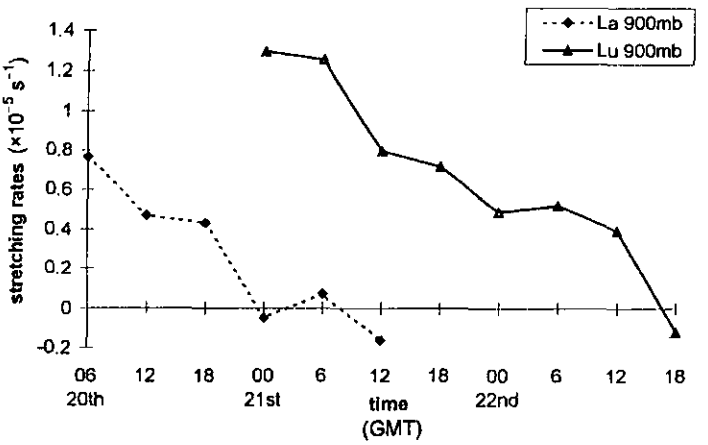

Figure 14. Along-front environmental-stretching rates at 900 mb for L_A and L_U of case (d) (see text). The plotted values are averages over the central half of the frontal box.

L_A for barotropic instabilities to play an important role. However, the increase in amplitude of L_A does coincide with a decrease in environmental along-front stretching (Fig. 14) which would allow barotropic instabilities.

Turning to L_U, Fig. 13 illustrates the relative strength of the vorticity strip at L_U through the examination period. The frontal cyclone undergoes a rapid amplification from 06 GMT to 12 GMT (21 January) with a more gradual increase over a further 24 hours. The increase in $W(\xi)$ is coincident with a decrease in the environmental along-front stretching of L_U (Fig. 14). The amplification of L_U occurs when $\partial v_e/\partial y_f$ falls from 1.2×10^{-5} s^{-1} to around 0.8×10^{-5} s^{-1}; this is towards the high end of the critical threshold zone for barotropic instabilities (cf. BT94II). What is striking is the temporal change in stretching of L_U—there is a clear change from high to low stretching over 24 hours. This is also true for L_{R1} in case (a) (see Fig. 6) and suggests that as well as the actual strain rate, the

temporal rate of change of strain may also be important. An extension of the BT94II model could be used to investigate this idea.

To investigate whether L_U was growing through barotropic processes the perturbation-wind derivatives $\partial v_i/\partial y_f$ and $\partial u_i/\partial y_f$ were examined (as described for case (a), Fig. 7). These showed the tilts with, and against, the vorticity-strip shear that are indicative of barotropic growth; however, the patterns were not as distinct as those in case (a). To ascertain whether baroclinic growth processes were present, cross-sections of PV along the front were examined (as described for case (b), see Fig. 9), and an along-front ('westerly') tilt with height was visible between the low-level L_U and the upper-level tropopause anomaly. However, the magnitude of the tilting PV anomaly was not that great (0.8 PVU). Note that the low-level PV strip had a maximum in the interior of the troposphere, around 1–2 km in height, and so internal baroclinic growth may also be occurring (cf. Charney and Stern 1962). It is not certain which of the above growth mechanisms were the most important for the amplification of L_U, and a more comprehensive examination is beyond the scope of this study. However, there is evidence of some barotropic edge-wave growth, which the drop in environmental stretching allowed to occur.

4. Discussion

To try and synthesize all the case-study analyses into an overall picture, a regime diagram has been developed. Figure 15 shows the rate of change of vorticity waviness ($dW(\xi)/dt$) against environmental along-front stretching ($\partial v_e/\partial y_f$) for all the cases investigated. The rate of change of $W(\xi)$ is a measure of the *growth* of a frontal cyclone. The along-front stretching rates are normalized by α_{min}, the minimum strain rate required to suppress all barotropic frontal-wave growth (cf. Eq. (8) and BT94II). This normalization accounts for the differing strengths of the vorticity strips in each case; clearly if the vorticity strip were not that anomalous then significant wave amplification through edge-wave dynamics could not be expected.

The regime diagram allows the testing of a hypothesis suggested by the theoretical modelling work of Dritschel *et al.* (1991), BT94II and Renfrew (1995). The hypothesis is that *sustained strong along-front stretching is a sufficient condition for barotropic frontal stability; weak along-front stretching is a necessary condition for barotropic frontal instability*. To test the hypothesis all the points from all the cases are plotted, except those points where the frontal cyclone has started to saturate through nonlinear processes, i.e. where the cyclone has left the developing stage (cf. Schär and Davies 1990; Malardel *et al.* 1993). This is judged to have happened if (i) the frontal cyclone has reached a finite amplitude size (defined by $W(\xi)$ greater than 1.0×10^{-4} s^{-1}), and (ii) the frontal cyclone is at the end of its life cycle ($W(\xi)$ is monotonically decreasing). This eliminates nine data points, leaving 20 points. The error bars indicate the maximum variation found in the sensitivity study of Renfrew (1995), where the frontal-box size and angle were varied by small amounts (see section 2). Note that the rate of change of $W(\xi)$ is calculated by differencing the 6-hourly sampled values (i.e. by differentiating the curves plotted in Figs. 5 and 13, for example). The corresponding $\partial v_e/\partial y_f$ is taken as the mean of the two stretching values of those times, normalized by α_{min}. The α_{min} is calculated for each time, with $2\mu = 0$ (i.e. infinite wavelength); recall this provides an upper bound for α_{min}. This means the *critical threshold* for barotropic-wave suppression is a normalized stretching rate of 1; *weak* stretching is less than 1, and *strong* stretching is greater than 1. To satisfy the hypothesis above, all the points in Fig. 15 should lie in either the lower right quadrant (strong stretching and no growth) or the upper left quadrant (weak stretching and growth), with the dividing line at 1.

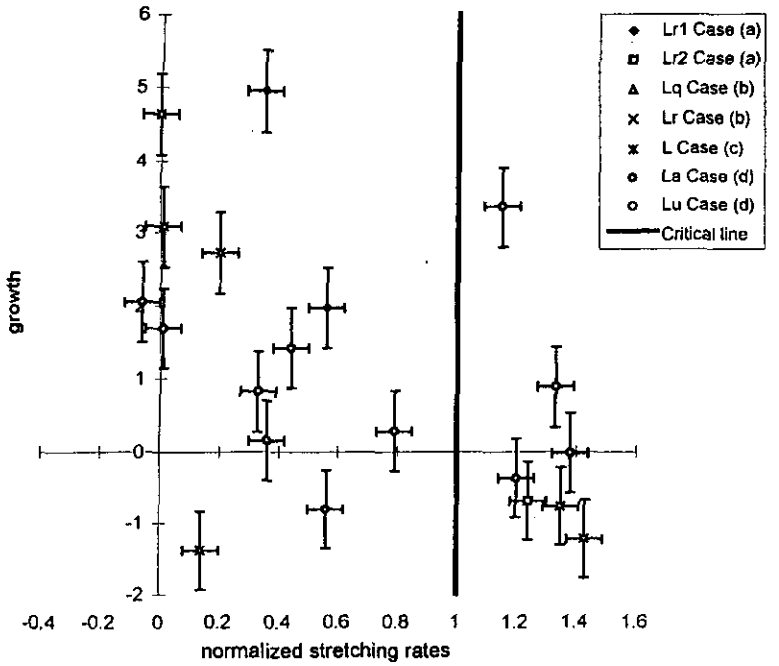

Figure 15. A regime diagram showing growth against along-front stretching. The growth is measured as the rate of change of vorticity waviness (units $\times 10^{-9}$ s^{-2}) and the stretching is measured as $\partial v_e/\partial y_f$ normalized by α_{min} (the critical threshold for suppression of all barotropic waves—see text for explanation). Data points are plotted for all four cases set out in the text. The error bars indicate the maximum errors found in the sensitivity study of case (a), as mentioned in section 2. In the upper right quadrant, waves are growing in weak environmental-stretching deformation; in the lower left quadrant wave growth is suppressed by the strong environmental-stretching deformation.

All but four points lie in these two quadrants. In the majority of the plotted times the cyclones are growing in an environment of weak stretching deformation. At five times (L_{R2} case (a), case (c) and two points from L_A case (d)) the cyclones are decaying in an environment of strong stretching deformation. There are two points in the lower left quadrant where the frontal cyclone has undergone a small decrease in amplitude, as measured by vorticity waviness; however, as illustrated in Fig. 13 (at 00 GMT for L_U case (d)), this is only a small decrease in an overall growth period. There are also two points (from L_U case (d)) in the upper right quadrant. These are from 03 GMT and 09 GMT 21 January, early in the growth phase of L_U. It was noted that the stretching was falling at these times, but was still large, suggesting the idea that the *temporal rate of change of stretching may be important*, as well as the actual stretching rate. This should be a topic for future research.

In conclusion, it appears the hypothesis relating barotropic frontal-cyclone growth and environmental stretching is largely borne out. The majority of data points fit the hypothesis with four exceptions. In dimensional units the theoretical critical threshold is in the range 0.5–1.2 $\times 10^{-5}$ s^{-1} for the analysed cases (taking $2\mu = 0$, i.e. an upper bound). For a front with typical-strength vorticity (an along-front average vorticity of about 1×10^{-4} s^{-1}), a critical threshold around 0.8×10^{-5} s^{-1} seems to fit the observed results.

5. Conclusions

It has become clear that the role of stretching deformation, due to the synoptic environment of a front, is crucial in the evolution of any instabilities on that front. A change of

stretching deformation over time, or location, can differentiate growth from suppression of frontal waves. For barotropic instabilities a hypothesis suggested by theoretical modelling work is largely borne out—as summarized in Fig. 15. If the stretching deformation of the front is strong (relative to the vorticity strip), then barotropic instabilities are unlikely to grow. If the stretching deformation of the front is weak, then barotropic instabilities will be free to grow, in the form of edge waves on a low-level potential-vorticity strip, if one exists. In certain cases the observed frontal-wind derivatives were examined and compared with theoretical model perturbation-wind derivatives, adding evidence that the frontal cyclone's growth was through barotropic edge-wave amplification.

In addition, this study has provided a range of values for the commonly prescribed deformation-frontogenesis parameter, α, by calculating the environmental along-front stretching $\partial v_e/\partial y_f$. The calculated α ranged from -0.5×10^{-5} s^{-1} to 1.6×10^{-5} s^{-1}. This is the same order of magnitude as the standard theoretical value (1.0×10^{-5} s^{-1}), but with a range that is significant for potential barotropic-instability growth and indeed frontogenesis models. A 2-level extension of the attribution technique (see the appendix) allowed the calculation of a range of values for the shearing-frontogenesis parameter, s^2, corresponding to an along-front temperature gradient of -0.4 K per 100 km to 0.1 K per 100 km, slightly less than the values generally taken in frontogenesis studies.

The attribution technique developed here is based on the vorticity and divergence attribution of Bishop (1996a, b) and so is suited to phenomena where two-dimensional vorticity dynamics are important; for example, when barotropic processes appear to play an important role, such as in secondary frontal cyclones or tropical cyclones. An interesting extension of the technique would be to examine vorticity on a (quasi-horizontal) isentropic surface. This would be appropriate for looking at upper-tropospheric levels where flow is generally on isentropic surfaces. In this case isentropic vorticity is the key quantity, and this is equal to potential vorticity, scaled by a density factor. This variant would be useful in examining the stability of upper-tropospheric PV tongues and filaments, such as those seen in high-resolution modelling studies (e.g. Methven 1996), and on a broader scale in forecast-model data (e.g. Hoskins *et al.* 1985).

The operational forecasting of secondary frontal cyclones is of great importance and, as discussed in the introduction and found by this study, the evolving synoptic environment of the front is crucial for frontal-cyclone development. Therefore, the modification of the techniques outlined in this study into an operational forecasting tool to assess this synoptic environment is of the utmost priority, and is currently being pursued by the authors.

Acknowledgements

The authors would like to thank Andy Macallan of the Joint Centre for Mesoscale Meteorology for assistance with obtaining the UK Meteorological Office data analysed in the study, and Raul Cunha at the University of Toronto for redrawing the pressure analyses. We would also like to thank Ted Shepherd and two anonymous reviewers for helpful comments on the first draft of this paper. Ian Renfrew was funded by a Natural Environment Research Council studentship during the course of this study which was completed at the University of Reading.

Appendix

Vorticity and divergence attribution can only be used on one level of data at one time. However, without knowing the vertical structure of a front it is not possible to establish the

amount of shear frontogenesis the front is undergoing. The classic Hoskins and Bretherton (1972) shear front has a prescribed *along-front* temperature gradient (equivalently a geostrophic vertical shear) given by the parameter $s^2 = -g/\theta_0 \cdot \partial\theta/\partial y_f$. This cannot be estimated by a single-level analysis as, if the temperature gradient is directly measured from observed data, local variations will mask the large-scale value. Hence, to measure s^2 accurately in real data the large-scale induced along-front temperature gradient must be found. To do this a 2-level attribution method is employed: the attribution method is carried out for the 900 mb and 700 mb levels, for example. Assuming a balance condition, it is possible to retrieve the geopotential, ϕ, corresponding to a certain wind field. For example, using geostrophic balance,

$$\phi = \frac{\psi}{f}, \tag{A.1}$$

where ψ is a stream function and f the Coriolis parameter (taken as constant). Differencing ϕ in the vertical via

$$\frac{\partial\phi}{\partial z} = \frac{g\theta}{\theta_0} = b \tag{A.2}$$

(assuming hydrostatic balance) will yield the potential-temperature field corresponding to that stream function. Unfortunately, when the stream function is found at more than one level an arbitrary constant renders the actual value of the geopotential or potential temperature meaningless. However, the main interests are the thermal gradients not the actual temperature itself; so, differentiating in the horizontal,

$$\frac{\partial}{\partial y_f}\left(\frac{\partial\phi}{\partial z}\right) = -\frac{g}{\theta_0}\frac{\partial\theta}{\partial y_f} \quad \text{and} \quad \frac{\partial}{\partial x_f}\left(\frac{\partial\phi}{\partial z}\right) = \frac{g}{\theta_0}\frac{\partial\theta}{\partial x_f}, \tag{A.3}$$

the unknown constants are dispensed with, and the temperature gradients are retrieved. If the total stream function is used in the balance approximation (A.1) then the full temperature gradients are retrieved. If the stream function due to non-frontal vorticity (ψ_e) is used in (A.1), then the environmental along-front and across-front temperature gradients are retrieved, as in section 3(*b*), so the prescribed values of s^2 in Hoskins and Bretherton (1972) or Keyser and Pecnick (1987) would be found. Note, there are several approximations used in the above method:

- Using only the stream function in the balance approximation means only considering the vorticity-induced winds. The much smaller divergence-induced winds are neglected. This is reasonable for a dominantly rotational flow.
- The simple geostrophic balance approximation $\phi = \psi/f$ is used, as one would expect the large-scale flow to be in approximate geostrophic balance, so, to find the large-scale temperature gradients, this balance is adequate. This is less justified in finding the frontal temperature gradients.
- Hydrostatic balance is employed. This is a negligible approximation given the above.

Note that the 2-level method requires the fronts to have a reasonably coherent vertical structure in vorticity. If cross-front thermal-wind balance is maintained then this will be the case, and in most observed fronts this appears accurate (see Thorpe and Clough (1991), for example). The 2-level approximation can be used to calculate measures of deformation and shearing frontogenesis based on the environmental winds and frontal temperature gradients, and frontal winds and environmental temperature gradients respectively—see Renfrew (1995) for details.

REFERENCES

Ayrault, F., Lalaurette, F., Joly, A. and Loo, C.	1995	North Atlantic ultra high frequency variability: An introductory survey. *Tellus*, **47A**, 671–696
Bell, R. S.	1994	'The assimilation of ERS-1 scatterometer winds'. Forecasting Research Division Technical Report, No. 89. Meteorological Office, Bracknell, UK
Bishop, C. H.	1993a	On the behaviour of baroclinic waves undergoing horizontal deformation. I: The '*RT*' phase diagram. *Q. J. R. Meteorol. Soc.*, **119**, 221–240
	1993b	On the behaviour of baroclinic waves undergoing horizontal deformation. II: Error-bound amplification and Rossby wave diagnostics. *Q. J. R. Meteorol. Soc.*, **119**, 241–267
	1996a	Domain independent attribution. I: Reconstructing the wind from estimates of vorticity and divergence using free space Green's functions. *J. Atmos. Sci.*, **53**, 241–252
	1996b	Domain independent attribution. II: Its value in the verification of dynamical theories of frontal waves and frontogenesis. *J. Atmos. Sci.*, **53**, 253–262
Bishop, C. H. and Thorpe, A. J.	1994a	Frontal wave stability during moist deformation frontogenesis. Part I: Linear wave dynamics. *J. Atmos. Sci.*, **51**, 852–873
	1994b	Frontal wave stability during moist deformation frontogenesis. Part II: The suppression of nonlinear wave development. *J. Atmos. Sci.*, **51**, 874–888
	1994c	Potential vorticity and the electrostatics analogy: Quasi-geostrophic theory. *Q. J. R. Meteorol. Soc.*, **120**, 713–731
Browning, K. A. and Roberts, N. M.	1994	Structure of a frontal cyclone. *Q. J. R. Meteorol. Soc.*, **120**, 1535–1557
Browning, K. A., Clough, S. A., Davitt, C. S. A., Roberts, N. M., Hewson, T. D. and Healy, P. G. W.	1995	Observations of the mesoscale substructure in the cold air of a developing frontal cyclone. *Q. J. R. Meteorol. Soc.*, **121**, 1229–1254
Charney, J. G. and Stern, M. E.	1962	On the stability of internal baroclinic jets in a rotating atmosphere. *J. Atmos. Sci.*, **19**, 159–162
Cullen, M.	1993	The unified forecast/climate model. *Meteorol. Mag.*, **122**, 81–94
Davis, C. A.	1992	Piecewise potential vorticity inversion. *J. Atmos. Sci.*, **49**, 1397–1411
Davis, C. A. and Emanuel, K. A.	1991	Potential vorticity diagnostics of cyclogenesis. *Mon. Weather Rev.*, **119**, 1929–1953
Dritschel, D. G.	1989	On the stabilization of a two-dimensional vortex strip by adverse shear. *J. Fluid Mech.*, **206**, 193–221
Dritschel, D. G., Haynes, P. H., Juckes, M. N. and Shepherd, T. G.	1991	The stability of a two-dimensional vorticity filament under uniform strain. *J. Fluid Mech.*, **230**, 647–665
Hewson, T.	1993	'The FRONTS '92 experiment: A quicklook atlas'. JCMM Internal Report No. 15, University of Reading, UK
Hoskins, B. J. and Berrisford, P.	1988	The storm of 15–16th October 1987: A potential vorticity perspective. *Weather*, **43**, 122–129
Hoskins, B. J. and Bretherton, F. P.	1972	Atmospheric frontogenesis models: Mathematical formulation and solution. *J. Atmos. Sci.*, **29**, 11–37
Hoskins, B. J., McIntyre, M. E. and Robertson, A. W.	1985	On the use and significance of isentropic potential vorticity maps. *Q. J. R. Meteorol. Soc.*, **111**, 877–946
Joly, A.	1995	The stability of steady fronts and the adjoint method: Nonmodal frontal waves. *J. Atmos. Sci.*, **52**, 3082–3108
Joly, A. and Thorpe, A. J.	1990	Frontal instability generated by tropospheric potential vorticity anomalies. *Q. J. R. Meteorol. Soc.*, **116**, 525–560
	1991	The stability of time-dependent flows: An application to fronts in developing baroclinic waves. *J. Atmos. Sci.*, **48**, 163–182
Keyser, D. and Pecnick, M. J.	1987	The effect of along-front temperature variation in a two-dimensional primitive equation model of surface frontogenesis. *J. Atmos. Sci.*, **44**, 577–604
Lynch, P.	1988	Deducing the wind from vorticity and divergence. *Mon. Weather Rev.*, **116**, 86–93
	1989	Partitioning the wind in a limited domain. *Mon. Weather Rev.*, **117**, 1492–1500

Malardel, S., Joly, A., Courbet, F. and Courtier, Ph.	1993	Nonlinear evolution of ordinary frontal waves induced by low-level potential vorticity anomalies. *Q. J. R. Meteorol. Soc.*, **119**, 681–713
Methven, J.	1996	'Tracer behaviour in baroclinic waves'. PhD Thesis, University of Reading
Morse, P. M. and Feshbach, H.	1953	*Methods of theoretical physics*, Vol. I and Vol. II. McGraw-Hill Book Co. Ltd
Polavarapu, S. M. and Peltier, W. R.	1993	Formation of small-scale cyclones in numerical simulations of synoptic-scale baroclinic wave lifecycles: Secondary instabilities at the cusp. *J. Atmos. Sci.*, **50**, 1047–1057
Renfrew, I. A.	1995	'The development of secondary frontal cyclones'. PhD Thesis, University of Reading
Schär, Ch. and Davies, H. C.	1990	An instability of mature cold fronts. *J. Atmos. Sci.*, **47**, 929–950
Thorncroft, C. D. and Hoskins, B. J.	1990	Frontal cyclogenesis. *J. Atmos. Sci.*, **47**, 2317–2336
Thorpe, A. J. and Clough, S.	1991	Mesoscale dynamics of cold fronts: Structures described by dropsoundings in FRONTS 87. *Q. J. R. Meteorol. Soc.*, **117**, 903–941